Measurement of OH radicals at state $X\,^2\Pi$ in an atmospheric-pressure micro-flow dc plasma with liquid electrodes in He, Ar and N_2 by means of laser-induced fluorescence spectroscopy

2012 J. Phys. D: Appl. Phys. 45 125201

(http://iopscience.iop.org/0022-3727/45/12/125201)

J. Phys. D: Appl. Phys. **45** (2012) 125201 (10pp) doi:10.1088/0022-3727/45/12/125201

Measurement of OH radicals at state $X\,^2\Pi$ in an atmospheric-pressure micro-flow dc plasma with liquid electrodes in He, Ar and N_2 by means of laser-induced fluorescence spectroscopy

L Li[1], A Nikiforov[1,2], Q Xiong[1,3], X Lu[3], L Taghizadeh[1] and C Leys[1]

[1] Department of Applied Physics, Research Unit Plasma Technology, Ghent University, Jozef Plateaustraat 22, Ghent B-9000, Belgium
[2] Institute of Solution Chemistry of the Russian Academy of Science, Academicheskaya St., 1, Ivanono 153045, Russia
[3] College of Electrical and Electronic Engineering, HuaZhong University of Science and Technology, WuHan, Hubei 430074, People's Republic of China

E-mail: anton.nikiforov@ugent.be

Received 8 December 2011, in final form 8 February 2012
Published 6 March 2012
Online at stacks.iop.org/JPhysD/45/125201

Abstract
The density of OH radicals in ground state is measured by laser-induced fluorescence (LIF) spectroscopy in the core of a micro-flow discharge in He, Ar and N_2 with a water electrode. The lines $P_2(6)$, $P_1(4)$ and $P_2(3)$ of the $X\,^2\Pi$ ($v'' = 0$) to the $A\,^2\sum^+$ ($v' = 1$) transition are used for OH radical excitation. The density of the main quencher of OH radical in the core of the discharge is estimated based on the time decay of the LIF signal. It is revealed that the plasma core consists of a high amount of 8–10% of water vapour. The calculation of the absolute density of OH radical is carried out based on the model of LIF excitation including vibrational and translation energy transfer, and the results in different gases are presented for the discharge.

(Some figures may appear in colour only in the online journal)

1. Introduction

Nowadays, atmospheric-pressure plasmas (APPs) attract a great deal of attention in different fields of science and technology [1, 2]. Whereas APPs are typically generated in gas mixtures containing noble gases or in ambient air, they can also be produced in bubbles in liquids or in the gas phase above a liquid surface. In recent years the interest in non-thermal plasmas in or in contact with liquids has increased significantly [3]. Unfortunately, there is still a lack of systematic investigations of the physics of plasma/liquid interface and data on absolute densities of species produced by plasma in contact with liquids. Intensive chemical reactions, energy transfer at the plasma–liquid interface and intensive evaporation make physics of these discharges very challenging but also allow one to generate a large number of active species: OH radicals, singlet oxygen, H_2O_2, O_3, etc. As a result, plasmas in or in contact with liquids are very effective for the treatment of many biological and chemical objects. Examples of applications include surgery [4], lithotripsy [5] and chemical analysis [6]. Among different types of plasmas in contact with water, a dc discharge above water surface is one having the advantage of easy optical access to the plasma, which is especially important for active laser diagnostics. A phenomenological study of dc excited electrical discharges between a metal pin and a water electrode has been done by many groups, e.g. by Gaisin and Son [7, 8] and recently by Bruggeman [3, 9]. This type of discharge is most often referred to as a glow discharge but also sometimes as a low-current arc discharge. A very similar system, which allows generation

of discharges in different gases, is a micro-flow discharge above water surface where composition of the gas phase can be controlled by external flow of the feed gas. Several groups performed the study of a micro-flow atmospheric-pressure glow discharge with liquid electrodes in various gases [10–12]. However, the study is mainly focused on the optical emission spectra of the discharges where only excited particles are accessible to this diagnostic. This is an important shortcoming, since the populations of the excited states are, as a rule, orders of magnitude lower than the ground state populations, and theoretical models have to be applied to provide the necessary link between the excited and ground states densities. Laser-induced fluorescence (LIF) spectroscopy is a technique that has direct access to ground state species populations [13]. LIF spectroscopy has been applied to numerous APPs and flames in order to measure absolute densities of active species: two-photon absorption LIF was used by Lukas *et al* [14] to detect N and O atoms in a DBD; also on a DBD, Ono *et al* [15] measured time behaviour of atomic oxygen density. One of the first published works on detection of hydroxyl radicals in high-pressure discharges using LIF was by Ershov and Borysow [16]; Ono and Oda also measured density of OH radicals and the gas temperature in an incipient spark-ignited hydrogen–air flame using predissociation fluorescence (LIPF) [17]. Recently in our group, OH radical density has been measured by the LIPF technique in an atmospheric-pressure glow discharge with liquid cathode and anode [18] where absolute density has been estimated based on the three-step model of Ono and Oda [17]. Unfortunately, the used model did not take into account the possibility of rotational/vibrational transfer on the OH state $A\,^2\sum^+$ ($v' = 1$) that can lead to inaccurate estimation of OH ground density.

This work deals with the measurement of the absolute densities of OH radicals by means of the LIF technique. The effect of the used gas on the generation of hydroxyl radicals in the positive column of the discharge is analysed and discussed for He, Ar and N_2 micro-flow discharges with liquid electrodes.

2. Experimental procedure

2.1. Micro-flow discharge above an electrolyte solution

The experimental set-up for LIF diagnostics is presented in figure 1. The used system is similar to that used recently for a glow discharge investigation [18]. A direct current discharge is generated between a metal electrode and a liquid surface (distilled water). A cone-shaped stainless steel metal electrode with a top angle of approximately 40° with a rounded and polished tip is attached to a micrometre screw above a liquid reservoir. The metal electrode has a narrow uptake with a diameter of 0.5 mm where the flow of gas (Ar or He purity 99.99%) with a flow rate of 300 sccm is applied. The distance between the metal electrode and the water surface is adjustable with a micrometre screw and is fixed as 8 mm. The volume of liquid in the reservoir is 0.5 l. The reservoir is refilled with distilled water before every experiment. A dc discharge is generated by applying a positive or negative high voltage (2.0–2.5 kV) to the metal electrode. A Technix HV1200 W power supply is used in current regulated mode and the applied current after breakdown of the gap is readjusted in order to reach a desirable value in the range 10–30 mA. A ballast resistor of 30 kΩ in series with the discharge is used for stabilization of the plasma and to limit the discharge current. A Tektronix P6005 1000 : 1 high-voltage probe is used to measure the applied voltage. The current is obtained by measuring the voltage across a shunt resistor in series with the setup.

2.2. Laser-induced fluorescence arrangement and optical emission spectroscopy

In this work we use the LIF technique based on excitation of hydroxyl radicals by means of the $X\,^2\Pi$ ($v'' = 0$) to the $A\,^2\sum^+$ ($v' = 1$) transition around 285 nm. A detailed description of the excitation and detection technique for the investigation of OH radical production in APPs by the LIF technique can be found elsewhere [15–20] and only a brief description of the used system is given here. As shown in figure 1(*a*), the Sirah Cobra-Stretch dye laser with a second harmonic generation (SHG) unit, pumped by a pulsed Nd : YAG laser, operating at its second harmonics excites the ground-state OH radicals ($X\,^2\Pi$, $v'' = 0$) to the ($A\,^2\sum^+$, $v' = 1$) by three lines $P_2(6)$, $P_1(4)$ and $P_2(3)$. The pathway of the laser beam is presented in figure 1(*b*). The linewidth of the dye laser is about 0.01 cm^{-1} and the pulse width is 8 ns. The maximum energy per pulse is 10 mJ and the laser beam has a rectangular shape with a cross-sectional area of $5 \times 1.5\ mm^2$ in the vicinity of the discharge. The energy of the beam can be attenuated down to 2 μJ using beam splitters and grey filters to reach conditions where the LIF signal depends linearly on the laser pulse energy. The fluorescence is collected at 8 cm from the positive column and led through an ultraviolet–visible optical fibre to a Hamamatsu R928 photomultiplier tube (PMT) after passing the optical bandpass filter with a central wavelength of 309 nm and spectral full-width at half-maximum (FWHM) of 10 nm. The LIF signal is accumulated by a SR430 photon counter at the frequency of the YAG : Nd laser during 1000 pulses. Calibration of the LIF signal is carried out by the commonly used Rayleigh scattering technique at the wavelength 309 nm [26] close to the maximum transparency of the filter.

The size of the positive column of the discharge is measured from the images of the discharge captured by a Hamamatsu ICCD camera (C8484) with the same UV filter as that used for the LIF. The overview emission spectra are obtained with an S2000 Ocean Optics spectrometer with a resolution of 1.2 nm in the range 280–900 nm. The high-resolution spectra (0.05 nm resolution) used for OH radicals' rotational temperature calculation are measured by means of an Avantes spectrometer. The rotational temperature (T_{rot}) of OH radicals is derived from the emission of the OH(A–X) (0–0) transition at 306–311 nm. In this case the method of Boltzmann plot is used [9] based on plotting $\ln(I\lambda/(2J+1)A_{J'J''})$ against the energy of the levels and where the slope of the curve allows measuring T_{rot}.

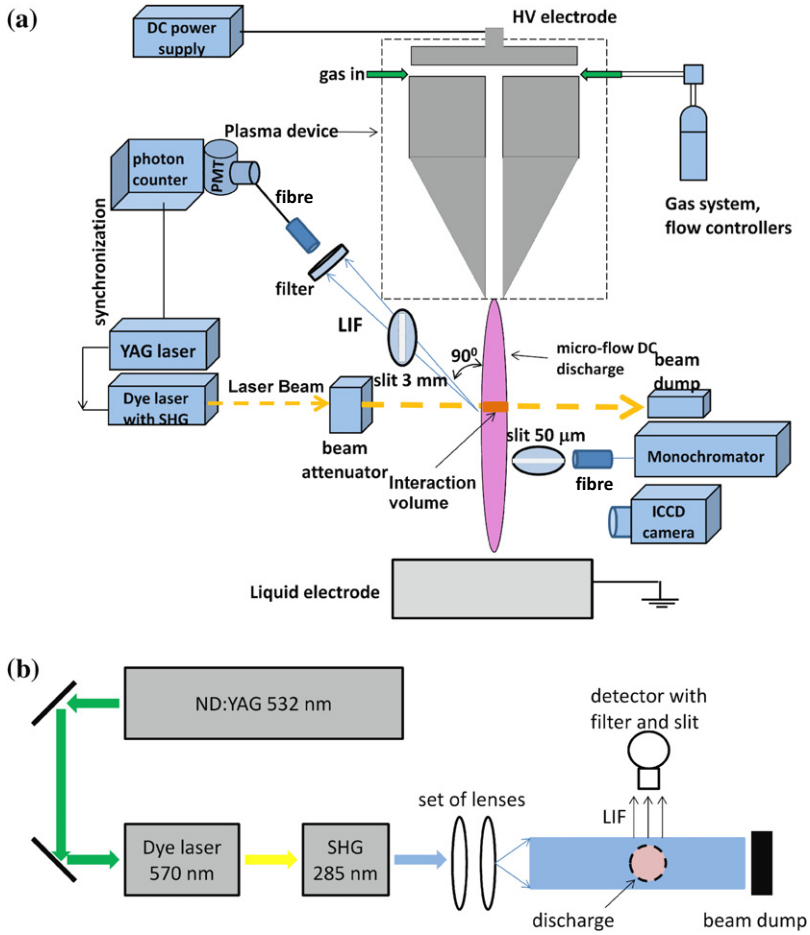

Figure 1. (*a*) Experimental set-up used for the measurements of OH radicals in a dc micro-flow discharge with liquid electrodes; and (*b*) laser pathway view.

3. LIF model

The interpretation of the LIF results requires an analysis of the number of processes leading to the generation of the experimentally registered signal. The model has to take into account not only the excitation of OH radicals by laser and radiative decay of the excited OH(A) state but also the quenching, dissociation of the excited state and vibrational (VET) and rotational (RET) energy transfer. The potential energy diagram of OH radicals [21] together with a number of processes included in the model of the LIF signal analysis is presented in figure 2.

Due to pumping of '2' levels of OH(A) state from ground state '1' of OH radicals by the laser pulse, overpopulation of the excited '2' level is observed. Depopulation of ground state density '1' can be expressed as

$$\frac{\mathrm{d}N_1(t)}{\mathrm{d}t} = -B_{12}I_\mathrm{L}N_1(t) + (A_{21} + B_{21}I_\mathrm{L})N_2(t) \qquad (1)$$

where I_L is the laser intensity, N_i is the density of radicals on the corresponding level and A_{ij}, B_{ij} are the Einstein coefficients of emission and absorption of the radiation.

Population of excited level '2' can be described as

$$\frac{\mathrm{d}N_2(t)}{\mathrm{d}t} = B_{12}I_\mathrm{L}N_1(t) - (L_2 + B_{21}I_\mathrm{L})N_2(t) \qquad (2)$$

where L_2 is the sum of rates of all loss processes leading to a decrease in the LIF signal—see figure 2. In the present model the following effects are included in the calculation:

predissociation when excited OH($A\,^2\sum^+$) can directly dissociate into O(^{1}D), O(^{3}P) and H(^{2}S); electronic quenching when the electronic energy of OH($A\,^2\sum^+$) is removed upon collision by heavy particles by the following mechanism:

$$\mathrm{OH}(A\,^2\Sigma^+) + M \rightarrow \mathrm{OH}^-(X\,^1\Sigma^+) + M^+ \rightarrow \mathrm{OH}(X\,^2\Pi_i) + M;$$

radiative decay; RET—the excited radicals will transfer energy to the adjacent lower and upper rotational levels with in the same vibrational band; and VET—the excited radicals will transfer energy to the adjacent lower vibrational level. Figure 2 describes such five decay processes. The effect of OH radical quenching is of key importance in the case of high-pressure plasmas where the decay time of the LIF signal will drastically decrease because of quenching, 10^{-9}–10^{-8} s^{-1} (depends on the quencher), when compared with the radiative lifetime of 700–800 ns. The effect of quenching of OH(A) by different colliders high-temperature media has been extensively studied by many groups [21, 23]. In the present model in order to carry out quantitative interpretation of the LIF signal the quenching effect is included in all kinetic equations describing the LIF signal decay based on experimental results of Keinle and others [23]. The laser excitation of certain rotational

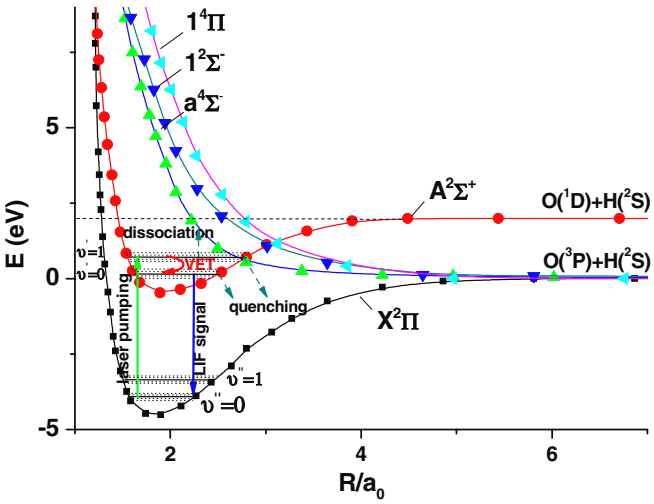

Figure 2. Potential energy curves for the first five electronic states of OH radicals and schematic of the processes included in the present LIF model. In the figure - vibrational levels · · · rotational levels. RET processes are not shown. The zero of energy corresponds to that of the ground states $O(^3P) + H(^2S)$.

transition from the ground state during a pulse of 8 ns results in the depopulation of the ground state density N_1 according to equation (5) and, in general, has to be considered in the model. In APPs this depopulation is compensated by fast RET processes having a rate constant Q_{RET} of $3.5 \times 10^{-9}\,\mathrm{s}^{-1}$ or higher [17, 18] which is sufficient to refill all rotational levels of the ground state during excitation and $N_1(t)$ can be considered as constant during the laser pulse. The same approximation has been used by others [15, 19] and gives very good agreement with experiment. Finally, from the LIF signal intensity I^0_{LIF}, calibrated in absolute units, the desired density N_1 can be obtained as

$$N_1 = \frac{G L_2 \int I^0_{\mathrm{LIF}}(t)\,\mathrm{d}t}{B_{12} I_{\mathrm{L}} \tau_{\mathrm{pulse}} V \sum_i t_{2i} A_{2i}} [1 + B_{12} I_L (L_2^{-1} + Q_{\mathrm{RET}}^{-1})] \tag{3}$$

where G is the efficiency of the optical system, V is the light-emitting volume and τ is the duration of the laser pulse. Usually a bandpass filter of 10 nm FWHM with a photomultiplier is used for registration of the signal and increasing the S/N (signal-to-noise) ratio especially when the intensity of the LIF signal is not strong enough. In our experiments, the registered LIF signal is the sum of intensities from several transitions appearing as LIF spectra because of RET and VET processes—see figure 2. Therefore, the sum $\Sigma t_{2i} A_{2i}$ is used in equation (3) to represent the distribution of all fluorescence transitions from level '2' to ground state and t_{2i} is the filter transmittance. In general, in the present model the sum $\Sigma t_{2i} A_{2i}$ can only be calculated if the temperature T_{rot} of OH radicals is known, e.g. from an independent measurement by optical emission spectroscopy (OES). The same temperature has to be used further for the evaluation of absolute ground density of OH radicals from the estimated value of N_1. It can be done if the rotational population distribution of OH radicals reaches an equilibrium described

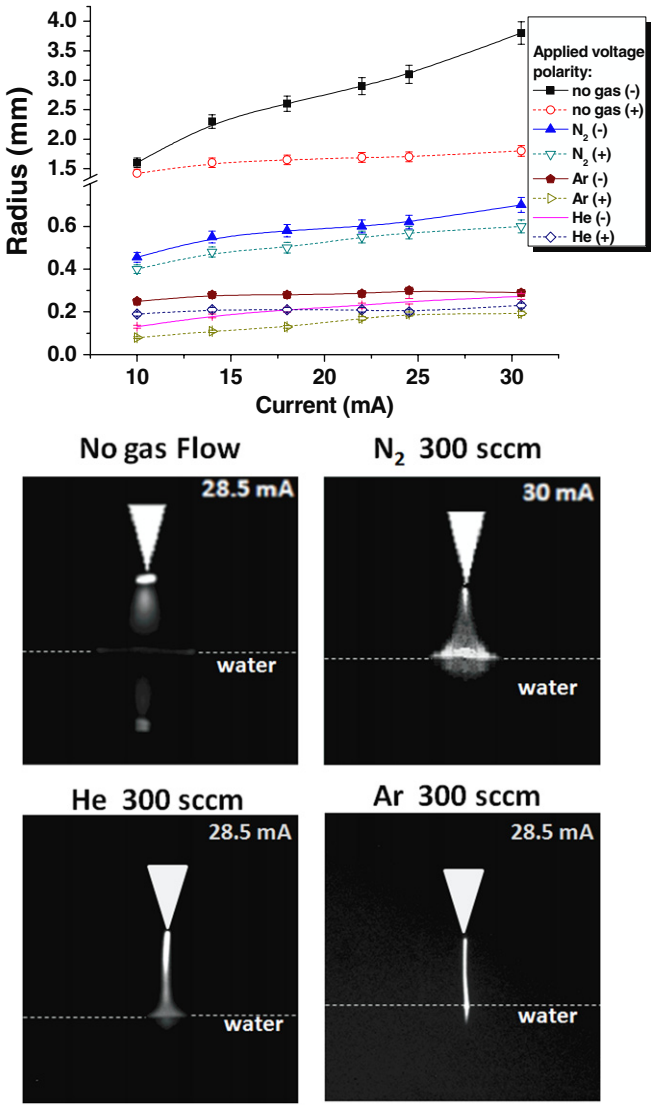

Figure 3. Radius of the discharge as a function of the discharge current. Images of the discharge through the UV 309 nm filter in He, Ar, N_2 and air (no gas flow) for negative applied voltage. The position of the electrode and surface of water are marked with white triangle and dashed line, respectively.

by the Boltzmann distribution. Hence, the absolute density of ground state $OH(X\,^2\Pi, v'' = 0)$ can be determined from N_1 density and rotational temperature T_{rot} of the radicals by [22]

$$N = \frac{N_1 \sum_i g_i \exp[-E_i/kT]}{g_1 \exp[-E_1/kT]} \tag{4}$$

where E_i and g_i are the energy and statical weight of the rotational level i.

4. Results and discussion

4.1. Emission spectroscopy of the discharge

The image of the discharge in all used gases at different applied currents and size of the positive column in the middle of the discharge gap is presented in figure 3. The discharge in N_2 and in air (without gas flow) is diffuse with distinguishing cathode

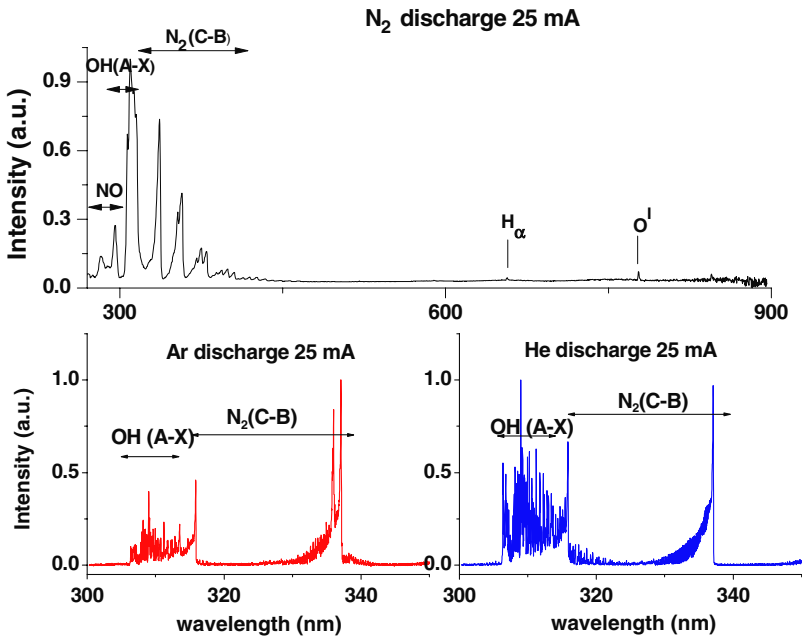

Figure 4. Overview of the discharge spectra in N_2 at 25 mA current with water as the cathode and high-resolution spectra in the range 300–350 nm for He and Ar discharges at 25 mA with water as the cathode.

space and positive column. The radius of the positive column is almost linearly dependent on the current and increases from 1.6 to 3.1 mm with an increase in the current from 10 to 30 mA in the case of negative polarity in the glow discharge without gas flow. For positive polarity when water is the cathode the radius of the discharge increases from 1.42 to 1.8 mm for the same current range. In the N_2 plasma the radius of the positive column in the middle of the gap is much smaller and it increases from 0.4 to 0.6 mm when water is used as the cathode and from 0.35 to 0.7 mm when water is the anode.

The discharge in noble gases (Ar and He) is constricted by comparing with the case of a glow discharge in molecular gases. Even at the highest current of 30 mA the radius of the plasma which is used further for the calculation of the absolute density of OH radicals is only 0.45 mm in He and 0.23 mm in Ar when water is the anode. Based on imaging of the discharge and also on the fact that V/I characteristics of the discharge in N_2 has a positive slope it was considered that the micro-flow discharge in N_2 is a glow-like discharge between pin and water in air. On the other hand, V/I characteristic of the discharge in He and Ar has a weak negative slope and no distinguishable separation on the cathode zone and positive column is observed. Correspondingly, the latter is considered as a low-current arc.

The rotational temperature T_{rot} of OH radicals required for interpretation of the LIF signal was measured by OES. An overview of the emission spectra of the discharge in N_2 with low resolution and parts of the spectra with a resolution of 0.05 nm (300–345 nm) in He and Ar are presented in figure 4.

All plasmas are characterized by significant amount of UV radiation in the range 280–312 nm mainly due to the presence of OH radicals, transitions $A\,^2\Sigma^+(v=0,1) \rightarrow X\,^2\Pi(v=0)$, intensive bands of the N_2 molecular system $N_2(C{-}B)$ and lines belonging to Ar and He. Weak O^I lines (777.4 843 nm) are registered in all gases as well. Only distilled water is used in the present experiments, so no traces of metals from the electrolyte were observed. The OH molecular band is used to estimate T_{rot}. As has been shown recently [3, 9] an APP in contact with water is characterized by a complicated scheme of OH radical production because of the possibility of H_2O excitation by electron impact with dissociation, by positive and negative ion recombination, etc. It results in non-Boltzmann behaviour of the OH radical rotational population at rotational numbers J higher than 13. It was suggested that a possible explanation of rotational population of OH radicals is the difference in the mechanisms of excited species generation. $OH(A)$ radicals are produced by electron impact excitation of ground state OH:

$$\mathrm{OH}(X\,^2\Pi) + \bar{\mathrm{e}} \rightarrow \mathrm{OH}(A\,^2\Sigma)^* + \bar{\mathrm{e}} \qquad (E_{\mathrm{threshold}} = 4\,\mathrm{eV}), \tag{5}$$

and by direct dissociation of water vapour:

$$\begin{aligned}\mathrm{H_2O}(X\,^1\mathrm{A_1}) + \bar{\mathrm{e}} &\rightarrow \mathrm{H_2O}(B\,^1\mathrm{A_1}) \\ &+ \bar{\mathrm{e}} \xrightarrow{\text{dissoc.}} \mathrm{OH}(A\,^2\Sigma)^{**} + \mathrm{H} + \bar{\mathrm{e}} \\ &(E_{\mathrm{threshold}} = 10\,\mathrm{eV})\end{aligned} \tag{6}$$

where $OH(A\,^2\Sigma)^{**}$ are radicals at highly excited levels. These two mechanisms are independent, which results in the overpopulation of rotational stages of $OH(A)$ with high rotational numbers, and only T_{rot} with $J < 13$ can be used as the rotational temperature of OH radicals. In this work we used the method suggested by Bruggeman [3] in order to estimate T_{rot}. For more details and explanations one can refer to the original work [3] and references therein. Figure 5 presents $\ln(I\lambda(2J+1)A_{JJ})$ for transition $OH(A\,^2\Sigma{-}X\,^2\Pi)$ as a function of levels' energy at $J < 13$, describing radical distribution among rotational levels for the discharge at 20 mA in three different gases.

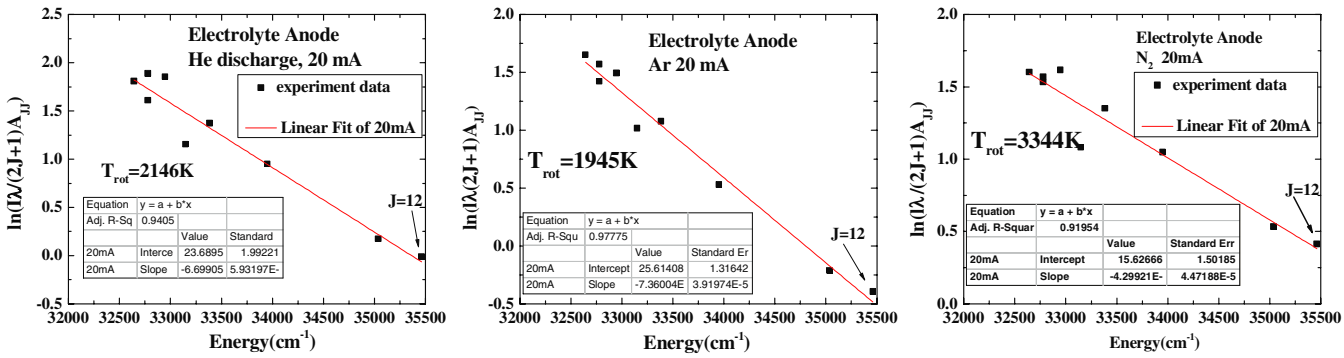

Figure 5. Boltzmann plot of the rotational distribution of OH(A) in the micro-flow glow discharge with water as the anode at a fixed flow rate of 300 sccm and fixed current of 20 mA.

Table 1. Rotational temperature of OH(A) as a function of the current for He, Ar, N_2 and glow discharge without gas flow estimated by the Boltzmann plot method. Error of the measurements is ±150 K.

		Current (mA)			
		10	18	26	30
Gas	Water polarity	Rotational temperature of OH(A) (K)			
He	Anode	2020	2148	2243	2325
	Cathode	1960	2075	2218	2275
Ar	Anode	1650	1810	1964	2040
	Cathode	1584	1652	1720	1750
N_2	Anode	2800	2893	3135	3115
	Cathode	2850	3045	3112	3250
No flow	Anode	3230	3355	3420	3480
	Cathode	3286	3320	3390	3370

The error of rotational temperature measurements is determined as ±150 mainly due to deviation of the spectral data from Boltzmann linear dependence at $J < 13$. The results of measurements for the case of water anode as well as water cathode at different currents are presented in table 1 where data for glow discharge without gas flow are presented for comparison as well.

The smallest temperature of about 1600 K is found in the Ar discharge and the highest temperature of around 3500 K is in the glow discharge without gas flow when water is the anode. In all gases $T_{\mathrm{rot}}^{\mathrm{OH}}$ is almost linearly dependent on the applied current. The presented data are in good agreement with the results of others [1, 3, 7, 9] where the gas temperature of the plasmas without gas flow is estimated by means of OES.

4.2. LIF measurements of OH radicals in the discharge

Typical time-resolved LIF signal for different currents and gases is presented in figure 6 where line $P_2(3)$ is used for excitation. The background due to plasma emission is taken into account and all data are reduced to 1 mJ of the beam energy. Data acquisition start by the photon counter (in figure 6 it is the 0 ns time point) corresponds to the TTL signal from the laser appearing before the laser pulse within 150–175 ns delay time. The latter slightly depends on the used Nd : YAG laser energy and is about 175 ns in the case of He discharge and only 155 in the case of Ar plasma which explains the small offset for He

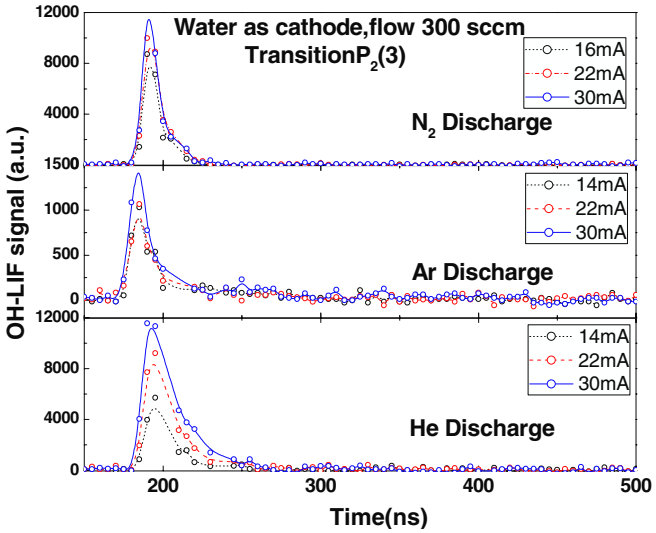

Figure 6. Time-resolved energy normalized LIF signal intensity (to laser energy 1 mJ) for the discharge in N_2, Ar and He as a function of the discharge current.

plasma in figure 6. However, for all calculations the presented time-resolved data were shifted to the point where the first LIF photons were registered by the photon counter and so the initial 155 (175 ns in the case of He plasma) were excluded from the analysis. The LIF signal which is proportional to the ground state radical density increases rapidly during the laser pulse with the maximum within 10–15 ns and decaying with a characteristic time of 30–50 ns (resolution of the registration system is 5 ns). Moreover a comparative increase in the LIF signal with increasing current is observed. The same tendency is also recorded for the case of water used as the anode. The high spectral resolution of the laser makes it possible to discriminate three different transitions of OH radicals by setting the laser wavelength to the maximum of specific transition. In figure 7(a) the laser scanned spectra of the three lines $P_1(4)$, $P_2(6)$ and $P_2(3)$ for the Ar discharge at 25 mA are presented. The measured signal is the integral LIF signal obtained with a PMT through an interference filter, whose transparency is plotted in figure 7(b). The filter is optimized to transmit the OH fluorescence from the $A\,^2\sum^+$ to $X\,^2\Pi$ band and eliminate the laser. As described in section 3 the density of OH radicals of the ground state is proportional to the measured

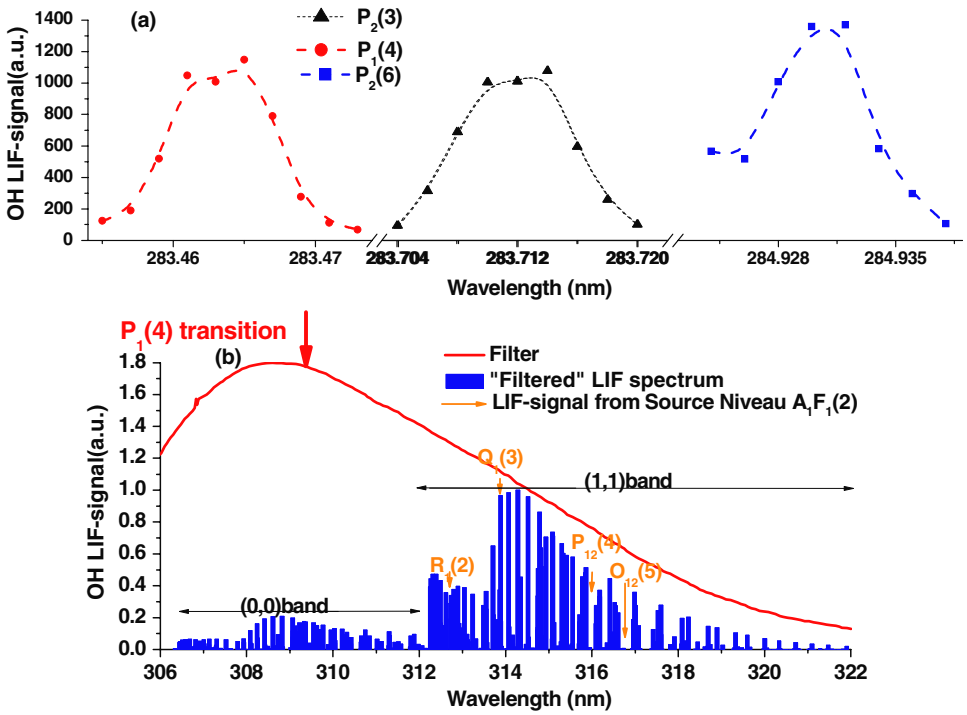

Figure 7. High-resolution laser scans of transitions $P_1(4)$, $P_2(6)$ and $P_2(3)$ for Ar discharge with water as the cathode at 25 mA discharge current. Stick spectra (*b*) at the bottom represent the results of the simulation of LIF spectra obtained for $P_1(4)$ excitation where the transparency of the interference filter is taken into account.

wavelength integrated fluorescence signal which is actually the spectra of laser-excited OH radical emission because of the RET and VET processes. In order to take into account all the processes forming the LIF spectra, we used LASKIN [23] to simulate the LIF spectra. In figure 7(*b*), sticks present such LIF spectra in the range 306–322 nm, obtained by multiplying the spectra from simulation by the filter transparency, for $P_1(4)$ excitation process. The marked lines were used for absolute density calculations with regard to equation (3) as will be shown later. The radiative decay time of excited OH radicals without quenching (e.g. in low-pressure flames or plasmas) can be estimated as 780–1500 ns depending on the transition, but due to the presence of different colliders (water vapour, N_2, O_2, O_3, OH) the LIF signal decay is much faster especially at atmospheric pressure. In the present experiments no effect of ozone on OH radical measurement was observed. In order to check ozone production by the glow discharge an independent experiment with ozone meter ('Envite') was carried out and very low ozone concentration close to the detection limit of the ozone meter in the range 1–2 ppm was detected for all used gases. The main reason for low ozone density is the fast thermal decomposition of ozone at high temperatures (>1500 K) and hence ozone interference with the LIF signal can be neglected. In the micro-flow discharge the main quencher will be the feed gas in the case of N_2 and H_2O in Ar/He because of the negligible low quenching rate of He and Ar. H_2O appears mainly in the core of the plasma because of thermal sputtering of the liquid electrode and ion bombardment of its surface. Based on the simulation of LIF signal with variation of H_2O content in gas phase we can estimate the density of H_2O in the plasma when best fitting of simulation and experimental decay presented in figure 6 is obtained. Figure 8 presents the typical results of simulation in LASKIN [23] with different content of H_2O in the positive column. The radiative decay time of OH radicals from ($A\,^2\sum^+$, $v' = 1$) strongly depends on the amount of water vapour even in the case of N_2 discharge despite the short decay time for pure N_2 compared with He and Ar. The best agreement is achieved with the range of 8% of H_2O in the positive discharge in He and 10% in Ar and also in N_2. The polarity of applied voltage has a negligible influence on the gas phase composition. An increase in current results in a very weak increase in H_2O in gas phase which is close to the statistical error of the measurements (15%). The measured H_2O content is in agreement with the result for the glow discharge above water obtained by the Rayleigh scattering technique [24] where the highest limit of H_2O density for a short gap of 3 mm, in contrast to 7 mm in the present work, is estimated as 30% (current 50 mA). Andre *et al* [25] estimated the upper limit of water content in the anode and cathode zones of the glow discharge in between two water layers as 25% and 45%, respectively. Smaller H_2O density of 10% measured in the present work can be explained by the fact that measurements were done in the positive column in contrast to the work of Andre *et al* [25] and also a gas flow was used which can decrease the H_2O density in the discharge. Based on the above-presented data, the ground-state OH density in the positive column of the discharge can be calculated when calibration of the detection system, e.g. by Rayleigh scattering, is carried out [18, 26]. The LIF model described in section 3 was used to calculate the ground-state OH absolute density. In order to avoid the calculation of the sum $\sum_i t_{2i} A_{2i}$ in equation (3) we rewrite part of it as

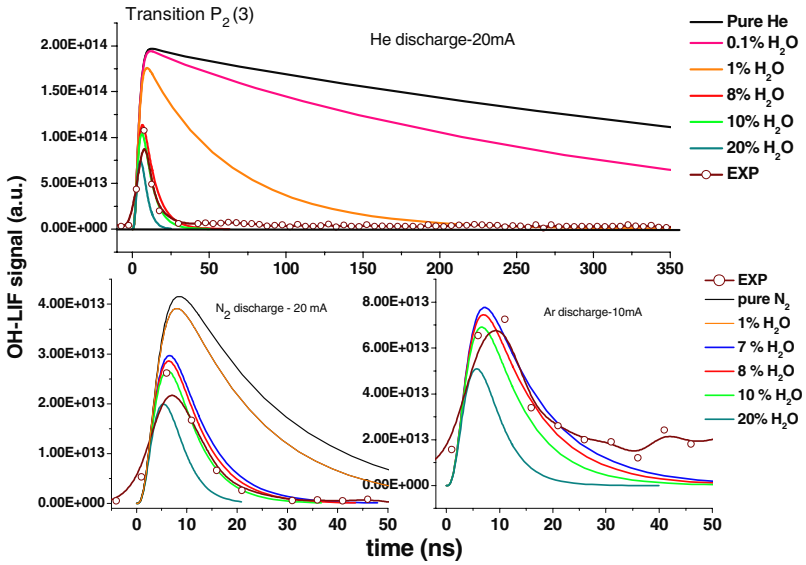

Figure 8. Comparison of the time evolution of the LIF signal with results of the simulation with different amounts of water vapour for the case of He discharge at 20 mA, N_2 discharge at 30 mA and Ar discharge at 10 mA, and water as the cathode.

$\frac{\eta_i \int I^0_{\mathrm{LIF}}(t)\,\mathrm{d}t}{t_{2i} A_{2i}}$ where $\eta_i \int I^0_{\mathrm{LIF}}(t)\,\mathrm{d}t$ is a fraction of the LIF signal corresponding to one specific transition from upper state 2 and can be found from the LIF spectra presented in figure 7 (e.g. one of the marked lines of the spectra at the bottom). The result of our calculation shows that the use of different radiative decay processes from upper state 2 will lead to exactly the same OH absolute density, so in all our calculations, we just use the decay process from upper state 2 with the strongest LIF intensity, e.g. for $P_1(4)$ excitation process, $Q_1(3)$ decay process from upper state $A_1F_1(6)$ is used for the calculation. All experiments are repeated for three laser excited transitions. Moreover, the excitation of different transitions leads to almost the same absolute density of OH radicals within an error of 10% which is close to the experimental error of 10–15%. The calculated ground state OH absolute density in the glow discharge in different gases with a liquid electrolyte, as anode and cathode, is shown for transition $P_2(6)$ as a function of discharge current in figure 9 together with the best polynomial fitting of the data. It has to be mentioned that the discharge in N_2 (both polarities) and in Ar (only negative polarity) at low currents of up to 18 mA is unstable and has the tendency of sparking. Correspondingly, for the N_2 plasma the first points at 16 and 18 mA are characterized by a large error of around 30–50% and are not presented for the Ar discharge at all. The density of OH radicals in the ground state almost monotonically increases with increasing discharge current from 10 to 30 mA for water as the anode, from 1.37×10^{20} to $1.8 \times 10^{20}\,\mathrm{m}^{-3}$ for the Ar discharge; from 6.15×10^{20} to $2.17 \times 10^{21}\,\mathrm{m}^{-3}$ for the He discharge and to $2.0 \times 10^{21}\,\mathrm{m}^{-3}$ for the N_2 discharge, while the density of OH radicals increases from 1.1×10^{20} to $2 \times 10^{20}\,\mathrm{m}^{-3}$ for the Ar discharge; from 5.7×10^{20} to $1.8 \times 10^{21}\,\mathrm{m}^{-3}$ for the He discharge and from 2×10^{21} to $2.3 \times 10^{21}\,\mathrm{m}^{-3}$ for the N_2 discharge when water is the cathode. The polarity of the applied voltage does not affect the density of OH radicals in the Ar plasma and has a weak effect in the case of He plasma and N_2 discharge. The plasma generated

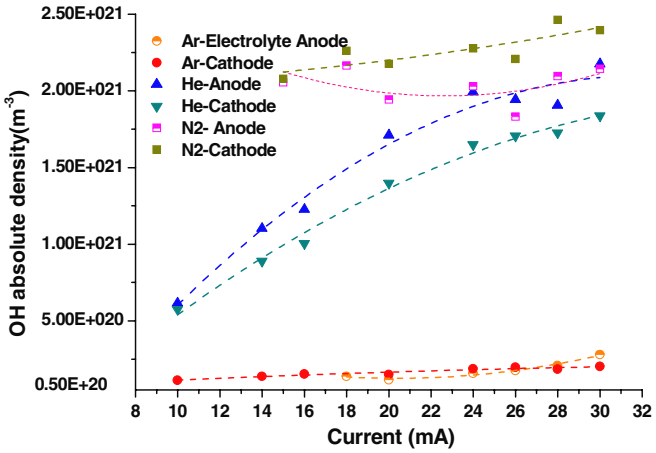

Figure 9. Absolute density of OH radicals in ground state generated in a micro-flow discharge with liquid electrodes in He/Ar/N_2 gases as a function of discharge current. Statistical error is 20%.

in N_2 is characterized by the highest OH density which is in agreement with our recent results [18] for a glow discharge in open air. The observed higher OH density at positive polarity for N_2 plasma is explained by the fact that the positive column when water is the cathode is constricted and therefore the current density is higher than in the case of water anode which leads to a higher ionization degree of the plasma and dissociation of H_2O. Remarkable difference in OH density between discharges in He/Ar and in molecular gas N_2 or in air [18] cannot be explained by electron dissociation of water or dissociative electron–ion attachment exponentially depending on the electron temperature. The former mechanism of OH production $e + H_2O \rightarrow OH + H + e$ [27] has a constant 2.3×10^{-12}–$1.8 \times 10^{-10}\,\mathrm{cm}^3\,\mathrm{s}^{-1}$ at $T_e = 1$–2 eV and for the latter $e + H_2O \rightarrow OH + H^-$ the constant is 4.9×10^{-18}–$4.7 \times 10^{-17}\,\mathrm{cm}^3\,\mathrm{s}^{-1}$ at the same electron temperature [27]. Following Raizer [28] a rough estimation of T_e can be done based on the equivalence of the rate of electron production

mechanisms to the rate of electron loss processes. The major mechanism of electron losses is dissociative recombination which is much faster than diffusion losses:

$$k_i N_e N \exp(-E_i/kT_e) - N_e N_+ k_d = 0$$

where k_i and k_d are the ionization and dissociative recombination rates, and N and N_+ are the density of neutral particles and positive ions, respectively. In the positive column, as a good approximation, $N_e = N_+$ can be used and k_d is around 10^{-14} m^3 s^{-1} [28]. The electron density of about (2–6) $\times$ 10^{20} m^{-3} estimated in [3, 9] leads to a T_e of around 1 eV in the case of Ar and $N_2$and a considerably higher T_e of around 2–2.5 eV in the case of He discharge. At such different T_e the reaction rates of OH production in the He plasma by the above-mentioned mechanisms should be at least 1.5 orders of magnitude faster [29]than in Ar or N_2 resulting in a higher OH density which is in disagreement with the experimental results presented in figure 9. The reason for higher content of OH radicals in the N_2 discharge can be thermal dissociation which starts to play an important role if T_g is higher than 2500 K [27, 29]:

$$H_2O + H_2O \rightarrow OH + H + H_2O,$$
$$k = 10^{-20}\text{–}4 \times 10^{-14}\,\text{cm}^3\,\text{s}^{-1}, \quad T_g = 2500\text{–}5000\,K$$

Both plasmas in He and Ar are characterized by T_g less than 2400 K at the highest current of 30 mA whereas in N_2 T_g is 2800 K even at a current of 10 mA, see table 1. Those high temperatures can explain the observed difference in OH radical density. Secondly, the possibility of OH(X) production in N_2 and air plasma should be noted because of the reaction [9, 31]: $N_2(A) + H_2O \rightarrow OH(X) + H + N_2(X)$. However, it was considered by the same authors that the rate of OH(X) generation by means of the presented reaction is too small in comparison with other possible mechanisms. Finally, it is important to note that the discharge in N_2 is glow whereas the Ar/He discharge is constricted without clear cathode or anode zone and is considered a low-current arc. Different modes of the discharge can change the mechanisms of OH radical production especially at the plasma/liquid interface. One of the possible reasons for the very low density of OH radicals of around 2 $\times$ 10^{20} m^{-3} in the Ar plasma can be not only low T_e and T_g but also depletion of Ar excited species in the core of the plasma. Recently, it has been shown [30] that in the core of a nonequilibrium atmospheric glow discharge in Ar generated by MW, the density of Ar excited species is depleted that can result in a decrease in the OH density produced in the core of the plasma especially because of the reaction [29] $Ar^m + H_2O \rightarrow OH + H + Ar$ ($K = 4.5 \times 10^{-16}$ m^3 s^{-1}). Unfortunately, experimental proof of the last statement required the knowledge of space-resolved OH density which is a plan for future work.

5. Conclusions

Absolute density of ground state OH(X) is measured in a micro-flow plasma with liquid electrodes in different gases by LIF spectroscopy. Discharge in He and Ar is a constricted low-current arc whereas the discharge in N_2 is diffuse similar to the glow discharge above water in air. Based on the developed LIF model the density of H_2O in the core of the plasma is estimated as 8–10% from the decay time of the LIF signal. Polarity of the applied voltage has negligible effect on the content of H_2O in the zone of positive column. The density of OH radicals is estimated from the calibrated LIF signal and it is linearly dependent on the applied current. The lowest value of OH density, 1.8×10^{20} m^{-3} (30 mA), is obtained in the Ar discharge whereas a higher OH density of about 2.2×10^{21} m^{-3} in the He plasma is probably because of the higher electron temperature which leads to a higher degree of H_2O dissociation. It was found that the most effective for OH radical production is a diffuse glow discharge in N_2 with a density of 2.3 $\times$ 10^{21} m^{-3} (30 mA, water as the cathode) mainly because of the fact that the higher temperature of gas phase leads to effective thermal dissociation of H_2O.

Acknowledgments

This work was supported by the Interuniversity Attraction Poles Program of the Belgian Science Policy (Project 'PSI'-P6/08) and by the China Scholarship Council (CSC).

References

[1] Fridman A, Chirokov A and Gutsol A 2005 *J. Phys. D: Appl. Phys.* **38** R1–24
[2] Becker K H, Schoenbach K H and Eden J G 2006 *J. Phys. D: Appl. Phys.* **39** R55–70
[3] Bruggeman P and Leys C 2009 *J. Phys. D: Appl. Phys.* **42** 053001
[4] Stalder K R, Mcmillen D F and Woloszko J 2005 *J. Phys. D: Appl. Phys.* **38** 1728–38
[5] Sunka P 2001 *Phys. Plasmas* **8** 2587–94
[6] Mitra B, Levey B and Gianchandani Y B 2008 *IEEE Trans. Plasma Sci.* **36** 1913–24
[7] Gaisin A F and Son E E 2005 *High Temp.* **43** 1–7
[8] Gaisin A F 2005 *High Temp.* **43** 680
[9] Verreycken T, Schram D C, Leys C and Bruggeman P 2010 *Plasma Sources Sci. Technol.* **19** 045004
[10] Shirai N, Ichinose K, Uchida S and Tochikubo F 2011 *Plasma Sources Sci. Technol.* **20** 034013
[11] Naoki S, Masato N, Shinji I and Ishii S 2008 *IEEE Trans. Plasma Sci.* **36** 1160–1
[12] Naoki S, Masato N, Shinji I and Ishii S 2009 *Japan. J. Appl. Phys.* **48** 036002
[13] Döbele H F, Mosbach T, Niemi K and Schulz-von der Gathen V 2005 *Plasma Sources Sci. Technol.* **14** S31–41
[14] Lukas C, Spaan M, Schulz-von-der-Gathen V, Thomson M, Wegst R, Döbele H and Neiger M 2001 *Plasma Sources Sci. Technol.* **10** 445
[15] Ono R, Yamashita Y, Takezawa K and Oda T 2005 *J. Phys. D: Appl. Phys.* **38** 2812
[16] Ershov A and Borysow J 1995 *J. Phys. D: Appl. Phys.* **28** 68
[17] Ono R and Oda T 2008 *Combust. Flame* **152** 69–79
[18] Nikiforov A, Xiong Q, Britun N, Snyders R, Lu X and Leys C 2011 *Appl. Phys. Express* **4** 026102
[19] Rothe E W, Gu Y, Chryssostomou A, Andresen P and Bormann F 1998 *Appl. Phys.* B **66** 251
[20] Ochkin V N 2009 *Spectroscopy of Low Temperature Plasma* (Weinheim: Wiley-VCH)
[21] Varandas A J C and Voronin A I 1995 *Chem. Phys.* **194** 91–100

[22] Huber K P and Herzberg G 1979 *Molecular Spectra and Molecular Structure: IV. Constants of Diatomic Molecules* (New York: Van Nostrand Reinhold)
[23] Rahmann U, Bulter A, Lenhard U, Dusing R, Markus D, Brockhinke A and Kohse-Hoinghaus K 2003 LASKIN—a simulation program for time-resolved LIF-spectra *Internal Report* University of Bielefeld, Faculty of Chemistry, Physical Chemistry
[24] Verreycken T, van Gessel A F H, Pageau A and Bruggeman P 2011 *Plasma Sources Sci. Technol.* **20** 024002
[25] Andre P *et al* 2002 *J. Phys. D: Appl. Phys.* **35** 1846–54
[26] Salmon J T and Laurendeau N M 1985 *Appl. Opt.* **24** 65
[27] Atkinson R, Baulch D L, Cox R A, Crowley J N, Hampson R F, Hynes R G, Jenkin M E, Rossi M and Troe J 2004 *Atmos. Chem. Phys.* **4** 1461–738
[28] Raizer Y P 1991 *Gas Discharge Physics* (Berlin: Springer)
[29] Bruggeman P and Schram D C 2010 *Plasma Sources Sci. Technol.* **19** 045025
[30] Miura N and Hopwood J 2011 *J. Appl. Phys.* **109** 113303
[31] Herron J T 1999 *J. Phys. Chem. Ref. Data* **28** 1453